Selectable Spontaneous Polarization Direction and Magnetic Anisotropy in $BiFeO_3-CoFe_2O_4$ Epitaxial Nanostructures

Nico Dix,[†,*] Rajaram Muralidharan,[†] Jose-Manuel Rebled,[†,‡] Sonia Estradé,[‡] Francesca Peiró,[‡] Manuel Varela,[§] Josep Fontcuberta,[†] and Florencio Sánchez[†,*]

[†]Institut de Ciència de Materials de Barcelona-CSIC, Campus de la UAB, 08193 Bellaterra, Spain, [‡]Departamento D'Electrònica, LENS-MIND-IN2UB, Universitat de Barcelona, c/Martí i Franquès 1, 08028 Barcelona, Spain, and [§]Departamento de Física Aplicada i Òptica, Universitat de Barcelona, c/Martí i Franquès 1, 08028 Barcelona, Spain

ABSTRACT We demonstrate that epitaxial strain engineering is an efficient method to manipulate the ferromagnetic and ferroelectric properties in $BiFeO_3-CoFe_2O_4$ columnar nanocomposites. On one hand, the magnetic anisotropy of $CoFe_2O_4$ is totally tunable from parallel to perpendicular controlling the $CoFe_2O_4$ strain with proper combinations of substrate and ferroelectric phase. On the other hand, the selection of the used substrate allows the growth of the rhombohedral bulk phase of $BiFeO_3$ or the metastable nearly tetragonal one, which implies a rotation of the ferroelectric polar axis from [111] to close to the [001] direction. Remarkably, epitaxy is preserved and interfaces are semicoherent even when lattice mismatch is above 10%. The broad range of sustainable mismatch suggests new opportunities to assemble epitaxial nanostructures combining highly dissimilar materials with distinct functionalities.

KEYWORDS: multiferroic nanostructures · $BiFeO_3$ · ferromagnetic spinels · magnetic anisotropy · epitaxial stabilization

The scarce number of room-temperature multiferroic materials hampers its potential in the development of novel devices, and two-phase nanocomposite thin films combining ferroelectric (FE) perovskite and ferromagnetic (FM) spinel phases[1−5] have emerged as a promising alternative to intrinsic multiferroics. Indeed, electric-field induced switching of magnetization has been observed, at room-temperature, in $CoFe_2O_4$ (CFO) nanopillars in $BiFeO_3$ (BFO) matrix deposited on $SrTiO_3$(001) (STO),[6−8] and it is believed that elastic interaction mediates the magnetoelectric coupling.[4] Bulk CFO is a FM spinel with cubic *Fm*3*m* structure ($a_{CFO} = 8.392$ Å), with the magnetic easy axis (EA) along ⟨100⟩ directions.[9] Bulk BFO is a FE with rhombohedral *R*3*c* structure (R-BFO) that can be described by a distorted perovskite cell with pseudocubic lattice, $a_{pc} = 3.96$ Å, and polar axis (*P*) along [111] of the pseudocubic cell.[2] Then, in nanocomposites on STO(001), the spontaneous polarization of BFO is at around 55° with respect to the normal direction, whereas in the CFO nanopillars the out-of-plane is the magnetic easy axis.[10−12] Clearly, the fixed directions of the FE and FM easy axes in a columnar nanocomposite restrict its development for optimal exploitation of both ferroic properties and magnetoelectric response. However, there is no such restriction in the case of BFO and CFO single phase (001)-oriented films, where the directions of the ferroic axes are selectable by appropriate substrate selection. Indeed, regarding BFO, the nearly tetragonal *P*4*mm* phase (T-BFO) can be epitaxially stabilized on suitable substrates,[13−16] and presents large spontaneous polarization nearly along [001].[17] Moreover, it has been recently observed that the structural transition between the R-BFO and T-BFO phases can be induced by an electrical field.[14,15] The subsequent cell deformation can largely modify the elastic coupling with neighboring CFO columns in nanocomposites, thus promising a stronger magnetoelectric response. Concerning single CFO films, the magnetic easy axis can be modified by using substrates of different lattice parameters.[18,19]

Therefore, the relative orientation of the distinct ferroic order directions could be tunable provided BFO−CFO columnar nanocomposites can grow epitaxially on suitable substrates, alternative to STO ($a = 3.905$ Å), allowing the growth of the desired phases and creating the necessary epitaxial strain to modify ferroic axes. However, the number of appropriate substrates to grow two-phase nanocomposites is much

*Address correspondence to ndix@icmab.es, fsanchez@icmab.es.

Received for review July 7, 2010 and accepted July 21, 2010.

Published online July 28, 2010.
10.1021/nn101546r

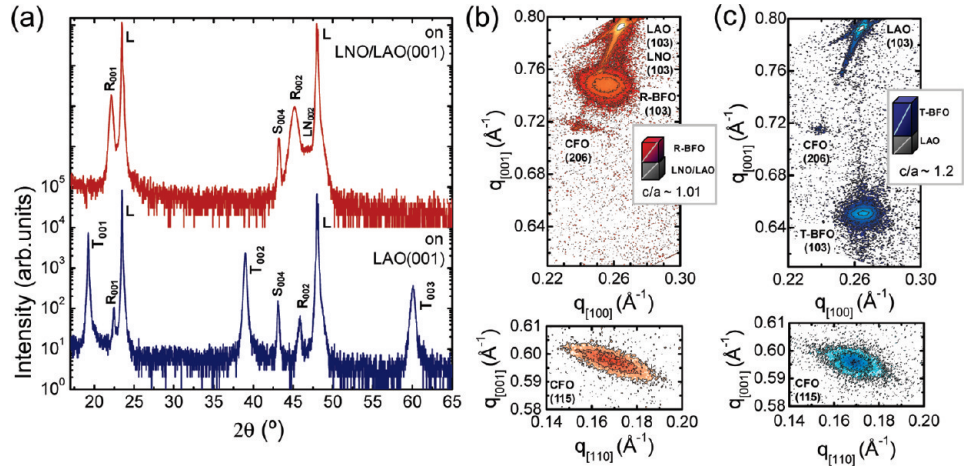

Figure 1. (a) XRD θ−2θ scans of BFO−CFO composite films on LNO/LAO(001) (top red curve) and LAO(001) (bottom blue curve). L, S, T, and R signal reflections from the substrate, spinel CFO, T-BFO, and R-BFO, respectively. XRD reciprocal space maps around LAO(103) for (b) BFO−CFO/LNO/LAO(001), and (c) BFO−CFO/LAO(001). Bottom panels show the corresponding maps around CFO(115).

reduced than that for single phase films, since all three lattice mismatches involved between the two ferroic materials and the substrate have to be considered. The mismatch of R-BFO with CFO ($f = (a_{R\text{-}BFO} - a_{CFO})/a_{CFO}$) is above 5%, and epitaxial growth could be compromised for one of them if the STO substrate is replaced (see Table ST1 of the Supporting Information). This is even more critical when considering the T-BFO phase ($a = 3.665$ Å, $c = 4.655$ Å) since its mismatch with respect to CFO is above 10% and thus the coherent or semicoherent state of the T-BFO/CFO interface, required for optimal elastic coupling, is challenging. Promisingly, the growth of spontaneous long-range phase ordering of other largely mismatched complex oxide BFO:Sm_2O_3 composites has been recently reported.[20,21]

In this article we will show that by appropriate substrate or buffer-layer selection for the growth of BFO−CFO, the polar direction of BFO can be rotated from [111] to nearly [001] while the orientation of the easy axis of CFO can be gradually modified, and thus the relative angle among the two polar axes can be varied. We deposited CFO−BFO nanocomposite films on (001)-$LaAlO_3$ (LAO) substrates and on $LaNiO_3$ (LNO) buffered LAO substrates, with pseudocubic lattice parameters $a_{LNO} = 3.86$ Å and $a_{LAO} = 3.79$ Å. We show that in spite of the large structural mismatch between the involved materials, both CFO and BFO phases grow epitaxially forming nanocomposites with well-defined CFO-nanopillar/BFO-matrix morphology. The matrix phase is R-BFO on LNO/LAO, whereas the metastable T-BFO phase is epitaxially stabilized on bare LAO. T-BFO/CFO interfaces are semicoherent, in spite of their large mismatch. CFO magnetic anisotropy critically depends on the lattice strain. Analysis of data corresponding to nanocomposites grown on other substrates and/or having other FE phases, evidence that the lattice strain and the magnetic anisotropy can be largely tuned by proper combination of substrate and FE phase.

RESULTS AND DISCUSSION

Figure 1a shows the XRD θ−2θ scans of nanocomposites on LNO/LAO(001) (top curve) and LAO(001) (bottom curve). The sample on LNO/LAO(001) presents reflections corresponding to CFO(001) and R-BFO(001), without traces of other orientations or phases. LNO reflections are not resolved because of the small thickness of the LNO buffer layer (around 10 nm) and the proximity of the substrate peaks.[22] The out-of-plane parameters of CFO and BFO are 8.364 and 4.019 Å, corresponding to compression of CFO and expansion of BFO. In contrast, in the nanocomposite directly grown on LAO, BFO grows, *c*-axis textured, in the quasi-tetragonal phase; only a few weak reflections of the rhombohedral phase are observed. T-BFO grows strained, with an out-of-plane parameter of 4.625 Å (*c* parameter of bulk T-BFO is 4.655 Å), whereas CFO is relaxed ($c = 8.391$ Å). It is worth mentioning that the nanocomposites on LAO(001) can only be obtained in a narrow substrate temperature window of 625−650 °C, very similar to that observed when growing nanocomposites on STO(001) substrates using equivalent deposition conditions.[23,24] XRD data of samples on LAO(001) deposited in the 600−700 °C range, evidencing BFO decomposition above 650 °C due to Bi loss, are included in Supporting Information (Figure S1).

XRD analysis of asymmetrical reflections confirmed epitaxial growth. The ϕ-scans around LAO(202), CFO(404), and R-BFO(202) of a nanocomposite film on LNO/LAO(001) as well as around T-BFO(202) on bare LAO(001) were measured. Each scan (see Figure S2 in Supporting Information) displays a set of four peaks, 90° apart, at the same ϕ angles, indicating [100]CFO(001)‖[100]LAO(001) and [100]R,T-BFO(001)‖[100]LAO(001) epitaxial relationships. Recip-

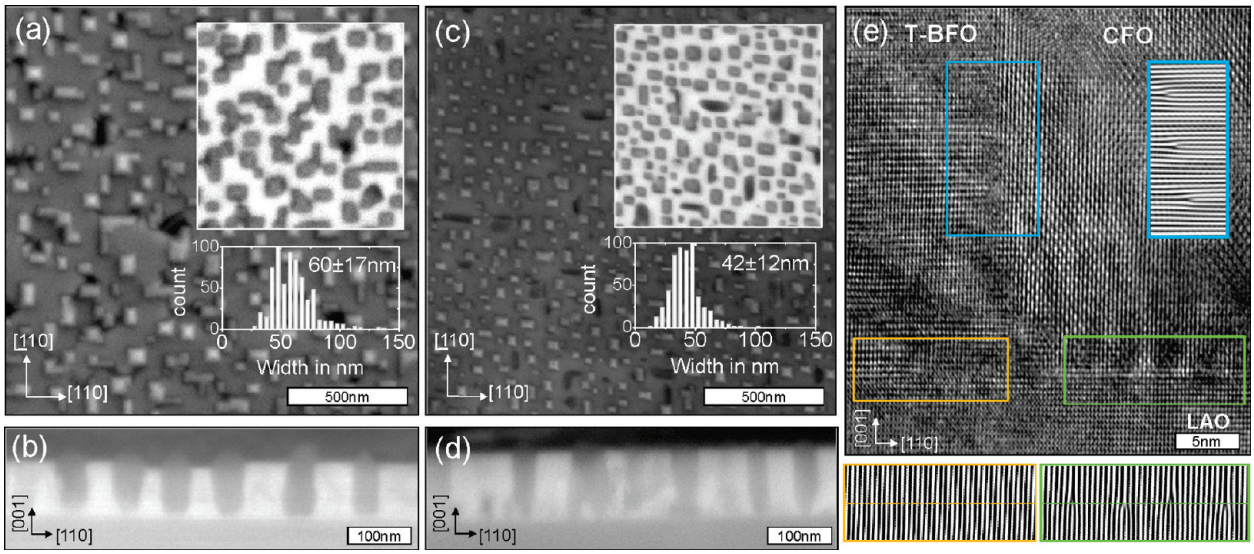

Figure 2. (a) SEM images (secondary electrons) of BFO−CFO on LNO/LAO(001). The area in the top right inset was imaged with backscattered electrons. Inset in the bottom right shows the histogram of the islands lateral size. (b) Cross-section view imaged with backscattered electrons. The corresponding images for the sample on bare LAO(001) are in panels c and d. (e) Cross section HRTEM image of the triple interface between a CFO nanopillar, the T-BFO matrix, and the LAO substrate. The continuity of planes between the T-BFO and LAO and the presence of dislocations at the CFO/LAO substrate interface and at the CFO/T-BFO lateral interface are revealed by FFT filtered images corresponding to the marked regions in the graph.

rocal space maps (RSM) around LAO(103) of films on LNO/LAO(001) and LAO(001) are presented in Figure 1b,c, respectively. The sample on LNO/LAO(001) shows a high intensity R-BFO(103) reflection, and in agreement with the symmetrical $\theta-2\theta$ scans, no T-BFO(103) peak is observed. The position of the R-BFO(103) reflection indicates partial strain relaxation ($a = 3.91$ Å, corresponding to in-plane strain $\varepsilon = -1.3\%$ and 70.6% of relaxation). In contrast, T-BFO on LAO(001) (Figure 1c) is fully strained ($a = 3.79$ Å, corresponding to $\varepsilon = 3.4\%$ and 0% of relaxation). The CFO(206) reflection is in both cases, barely observable due to its low intensity and the proximity of the K_β component of the substrate reflection. Alternatively, corresponding CFO(115) asymmetrical reflections are presented in the bottom panels of Figure 1b,c.

The surface morphology of the nanocomposites on LNO/LAO(001) and LAO(001) is presented in Figure 2 panels a and c, respectively. The secondary electrons (SE) images show faceted islands perfectly oriented along ⟨110⟩ in-plane directions; the majority of them have a square base and likely they have pyramidal shape; some few others islands are of hut-cluster type. The mean lateral size is ~60 nm on LNO/LAO(001) and ~42 nm on LAO(001) (see the histograms in the inset). Backscattered electrons (BSE) images were acquired simultaneously (see the insets in the top right). The BSE signal is of higher intensity in the areas where Bi is present (atomic number $Z_{Bi} = 83$ is much higher than $Z_{Fe} = 26$ and $Z_{Co} = 27$). It is observed that Bi is only present in the flat areas, implying that islands correspond to the CFO phase surrounded by a BFO matrix, being R-phase on LNO/LAO(001) and T-phase on LAO(001). The morphology in both cases is thus similar to that of nanocomposites on STO(001) substrates.[3,7,8,12,23,25] However, whereas BFO−CFO nanocomposites on LAO(001) and buffered-LAO(001) substrates show highly uniform and a flat BFO matrix, the BFO matrix of the nanocomposites grown on STO forms plateaus of different heights (see for example refs 8 and 23). The columnar structure of CFO is confirmed by cross sectional SEM analysis. The corresponding BSE images (Figure 2b,d) reveal the nanopillars topology of CFO (dark regions) in the R- or T-BFO matrix (bright regions). More detailed characterization of the T-BFO matrix/CFO nanopillar interfaces in the sample on LAO was conducted by cross-section high-resolution transmission electron microscopy (HRTEM). Figure 2e shows a cross-section micrograph and Fourier-filtered images corresponding to the three interfaces. CFO presents well-defined interfaces with both LAO substrate and T-BFO matrix, with misfit dislocations, approximately 5 nm apart. The interfaces are thus semicoherent: there are extra atomic planes in CFO in its interface with T-BFO matrix (≈10% tensile stressed, $a_{CFO}/2 < c_{T\text{-}BFO}$) and there are extra atomic planes in LAO in its interface with CFO (≈10% compressively stressed, $a_{CFO}/2 > a_{LAO}$). The other interface, between T-BFO and the LAO substrate, is fully coherent. It is noted that the epitaxial stabilization has occurred in spite of the important mismatch (−3.3%, tensile stress). In contrast, we find that BFO decomposes when composites are grown on substrates with large lattice parameters as $MgAl_2O_4$ ($a = 8.031$ Å) and MgO ($a = 4.212$ Å), causing epitaxial tensile stress to R-BFO. Probably, the better matching of the resulting Fe_xO_y oxides with these substrates favors the decomposition. As a result, Bi-rich dendritic structures are present on the surface, while the rest is covered by pyramidal

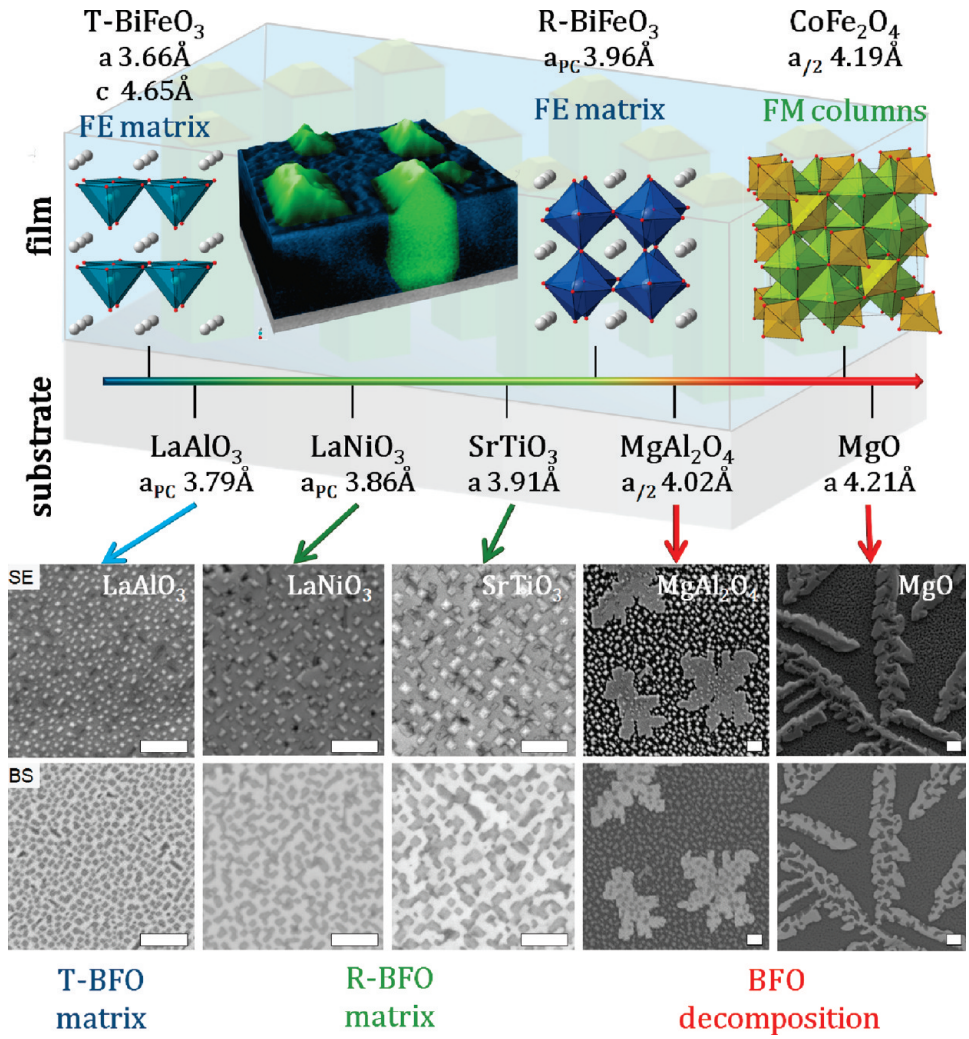

Figure 3. (top) Sketch shows the T-BFO, R-BFO, and CFO crystal structures and the topology of a sample grown on LNO. The 3D view is a result of combining different filtered SEM images. (bottom) Scanning secondary electrons images (SE) and backscattered electron images (BS) are shown for samples of 100 nm thickness grown under similar conditions on cubic substrates with increasing lattice parameter LAO, LNO/LAO, STO, $MgAl_2O_4$, and MgO. Films grown on LAO, LNO/LAO, and STO have a closed BFO matrix with surrounded CFO columns. In contrast, BFO decomposes on substrates causing tensile strain on R-BFO ($MgAl_2O_4$ and MgO), forming Bi-rich dentritic structures and pyramidal CFO islands. (scale bars are 500 nm).

objects typical for spinel phases (see SEM images in Figure 3, bottom).[26] The figure summarizes the impact of the substrate on the growth of BFO: as the substrate lattice parameter increases BFO changes from T-phase (on LAO) to R-phase (on LNO and STO), and finally decomposes (on $MgAl_2O_4$ and MgO). The top panel of Figure 3 shows the T-BFO, R-BFO, and CFO crystal structures and the topology of the nanocomposite deposited on LNO (the image is created combining filtered SEM images).

Room-temperature magnetization loops of the films on LNO/LAO and LAO are shown in Figures 4 panels a

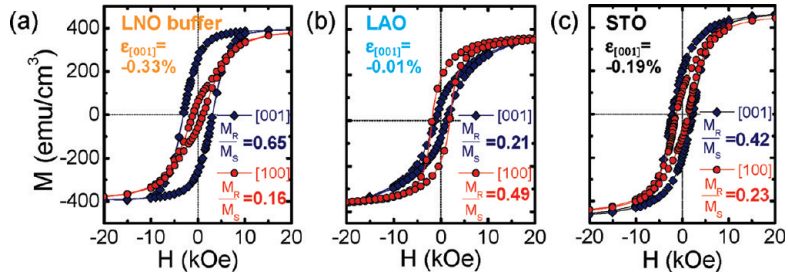

Figure 4. Magnetization hysteresis loops measured at room temperature with the field applied in the plane (circles) and out-of-plane (rhombi) for samples on (a) LNO/LAO(001), (b) LAO(001), and (c) STO(001). Magnetization is normalized to the CFO volume fraction. Labels in each panel indicate remanence/saturation magnetization ratio for parallel and perpendicular applied field.

and b, respectively. Measurements have been performed with the magnetic field applied perpendicular (rhombi) and parallel (circles) to the surface of the substrate, that is, along the [001] and [100] LAO axes. The magnetization has been calculated using the volume fraction of the CFO (38 vol %) and yields a saturation value of $M_S \approx 400$ emu/cm^3 for films grown either on LAO(001) (Figure 4b) or on LNO/LAO(001) (Figure 4a). This saturation magnetization matches very well with the reported bulk value. For completeness, we include here (Figure 4c) the magnetization loops of a nanocomposite deposited on the usual STO(001) substrates, having a quite similar M_S value.

However, although all films display a similar saturation, their magnetic anisotropy is markedly different. Whereas the out-of-plane direction is the easiest magnetic axis of CFO in films on LNO/LAO (Figure 4a), the in-plane direction is the easy-axis in the films on LAO (Figure 4b). The films on STO (Figure 4c) are somehow intermediate, although the out-of-plane direction is still favored. The distinct magnetic anisotropy is better quantified by the different magnetization remanence/saturation (M_R/M_S) ratios or more simply by the $M_R[001]/M_R[100]$ which gives 4.06, 0.43, and 1.82, respectively for films on LNO/LAO, LAO, and STO. It is illuminating to notice that the $M_R[001]/M_R[100]$ ratio has a clear correspondence with the strain state of the film as reflected by the ε value, included in each panel, as determined from the measured *c*-axis lengths. These data show that the in-plane magnetic easy axis is obtained for the film grown on LAO, which has the smaller strain ($\varepsilon \approx -0.01\%$), whereas out-of-plane magnetization develops with increasing strain from films on STO to films on LNO/LAO ($\varepsilon \approx -0.19\%$ and -0.33%, respectively).

Because of its large magnetostriction of CFO, strain plays an important role on the magnetic anisotropy of films. Indeed, in pure CFO films under tensile strain, that is, compressed out-of-plane cell parameter, the [001] direction is an easy axis, whereas (001) is an easy-plane in the case of opposite or negligible strain.[18,19] Our results for CFO in CFO−BFO nanocomposites follow exactly the same pattern. The agreement extends beyond the results presented here.

Indeed, in Figure 5 we collect the $M_R[001]/M_R[100]$ ratio for the films described here and we also include the results we have obtained on a number of other (001)-oriented epitaxial nanocomposites having distinct strain state. Data correspond to BFO−CFO nanocomposites deposited in similar conditions on bare STO(001) or $La_{2/3}Ca_{1/3}MnO_3$ buffered STO(001) substrates, and also from $BaTiO_3$−CFO nanocomposites on STO(001) (information about growth conditions and characterization can be found in ref 27). In addition, we also include in Figure 5 data from literature corresponding to BFO−CFO, $BaTiO_3$−CFO, and $PbTiO_3$−CFO nanocomposites.[1,10−12,28−30] (see Table ST2 of the Supporting Information for information on these films and

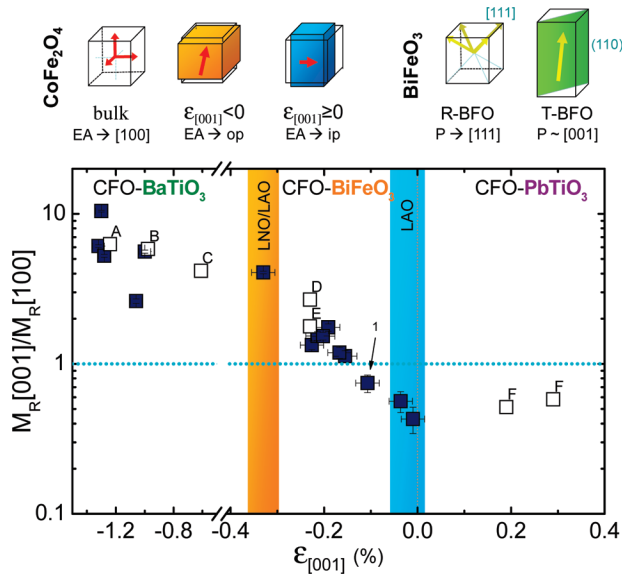

Figure 5. The $M_R[001]/M_R[100]$ remanence is plotted *vs* CFO out-of-plane strain. Solid symbols correspond to BFO−CFO and $BaTiO_3$ samples grown in our laboratory on STO(001), except the sample labeled with number "1" that was grown on $La_{2/3}Ca_{1/3}MnO_3$/STO(001). Capital letter labeled empty symbols correspond to values retrieved from literature: (A) ref 28, (B) ref 1, (C) ref 29, (D) ref 10, (E) ref 12, and (F) ref 30. Simplified sketches indicating the dependences of the CFO strain and the BFO phase on the directions of the magnetic easy axis and the spontaneous polarization, respectively, are plotted in the top of the Figure.

references). Data in Figure 5 display a clear trend. It evidences the dominating influence of the strain on the magnetic anisotropy of CFO in nanocomposites: highly *c*-axis compressed CFO in $BaTiO_3$ matrix shows highest perpendicular anisotropy, *c*-axis expanded CFO in $PbTiO_3$ matrix shows in-plane easy-axis, and CFO in BFO matrix is situated in between these extremes. Thus, the magnetic anisotropy is tunable from perpendicular to in-plane by the combined action of epitaxial strain induced by the substrate and the accompanying FE phase (see the sketch in Figure 5).

On the other hand, we have demonstrated here that the substrate selection determines which BFO phase (T or R) forms in the nanocomposite, thus critically affecting the corresponding FE properties. More precisely: the [001] crystal axes of both BFO phases in the nanocomposites are parallel to the [001] substrate direction and the direction of the spontaneous polarization depends on the specific phase of BFO (see the sketch in Figure 5), being almost parallel to the [001]LAO direction or at about 55° away from it for T-BFO[17] and R-BFO, respectively.

CONCLUSIONS

We have shown that exploitation of a large mismatch in heteroepitaxy of biferroic composites allows a dual selectivity on the orientation of both ferroic orders, offering new possibilities in their functional development. First, the magnetic anisotropy of CFO in biferroic nanocomposite thin films is dominated by the

magnetoelastic contribution. The CFO magnetic easy axis can be controlled, from out-of-plane to in-plane, by proper selection of the substrate and the FE phase. Second, the role of the substrate is also crucial on the epitaxial stabilization of rhombohedral or the nearly tetragonal phases which implies a rotation of the spontaneous polarization from [111] toward the normal [001] direction. Therefore, the relative direction of the magnetic anisotropy and the polarization axes can be selected and tuned. As both the magnetostriction of CFO and the polarization BFO largely depend on which phase or texture has been selected, larger strain-mediated magnetoelectric effects can be envisaged in optimized nanocomposites.

EXPERIMENTAL SECTION

Pulsed Laser Deposition. Nanocomposites with thickness around 100 nm were deposited at a rate of ~0.9 Å s^{-1} on LAO(001), LNO/LAO(001), and STO(001) at 625 °C substrate temperature by pulsed laser deposition (KrF excimer laser, 5 Hz repetition rate) using a $Bi_{1.1}FeO_3-CoFe_2O_4$ target with molar ratio of 65:35. The LNO buffers, around 10 nm thick, were deposited at 600 °C under an oxygen pressure of 0.1 mbar.

XRD. The crystal structure was analyzed by X-ray diffractometry (XRD) using Cu Kα radiation and the lattice parameters were calculated from the position of the diffraction peaks. Reciprocal space maps and pole figures have been acquired using Bruker D8 Advance diffractometer with area detector.

SEM. The morphology of the samples and the microstructure using cleaved cross sections along [110] substrate directions were measured using a Fei Quanta 200EF microscope equipped with a backscattering electron and EDX detector.

TEM. A sample on LAO substrate was prepared in cross section geometry for transmission electron microscopy and was studied in a Jeol J2010F microscope with a field emission gun operating at 200 kV.

Magnetic Measurements. Magnetization loops were measured by SQUID MPMS7XL at a temperature of $T = 300$ K.

Additional experimental details on sample preparation and characterization are reported elsewhere.[7,23,24]

Acknowledgment. Financial support by the Spanish Government (Projects: MAT2008-06761-C03, Nanoselect CSD2007-00041 and Consolider CSD2009-00013) and Generalitat de Catalunya (2009 SGR 00376 and CTP2009-00018) is acknowledged.

Supporting Information Available: Tabulated misfit parameters for all constituent phases and substrates, table for magnetization values extracted from literature, XRD θ/2θ patterns of T-BFO−CFO vertical nanocomposite *vs* growth temperature, XRD texture, and epitaxial analysis. This material is available free of charge *via* the Internet at http://pubs.acs.org.

REFERENCES AND NOTES

1. Zheng, H.; Wang, J.; Lofland, S. E.; Ma, Z.; Mohaddes-Ardabili, L.; Zhao, T.; Salamanca-Riba, L.; Shinde, S. R.; Ogale, S. B.; Bai, F.; *et al*. Multiferroic $BaTiO_3-CoFe_2O_4$ Nanostructures. *Science* **2004**, *303*, 661–663.
2. Ramesh, R.; Spaldin, N. A. Multiferroics: Progress and Prospects in Thin Films. *Nat. Mater.* **2007**, *6*, 21–29.
3. Yan, L.; Yang, Y.; Wang, Z.; Xing, Z.; Li, J.; Viehland, D. Review of Magnetoelectric Perovskite-Spinel Self-Assembled Nanocomposite Thin Films. *J. Mater. Sci.* **2009**, *44*, 5080–5094.
4. Nan, C. W.; Bichurin, M. I.; Dong, S.; Viehland, D.; Srinivasan, G. Multiferroic Magnetoelectric Composites: Historical Perspective, Status, and Future Directions. *J. Appl. Phys.* **2008**, *103*, 031101.
5. Levin, I.; Li, J.; Slutsker, J.; Roytburd, A. L. Design of Self-Assembled Multiferroic Nanostructures in Epitaxial Films. *Adv. Mater.* **2006**, *18*, 2044–2047.
6. Zavaliche, F.; Zheng, H.; Mohaddes-Ardabili, L.; Yang, S. Y.; Zhan, Q.; Shafer, P.; Reilly, E.; Chopdekar, R.; Jia, Y.; Wright, P.; *et al.* Electric Field-Induced Magnetization Switching in Epitaxial Columnar Nanostructures. *Nano Lett.* **2005**, *5*, 1793–1796.
7. Dix, N.; Muralidharan, R.; Guyonnet, J.; Warot-Fonrose, B.; Varela, M.; Paruch, P.; Sánchez, F.; Fontcuberta, J. On the Strain Coupling across Vertical Interfaces of Switchable $BiFeO_3-CoFe_2O_4$ Multiferroic Nanostructures. *Appl. Phys. Lett.* **2009**, *95*, 062907.
8. Yan, L.; Xing, Z.; Wang, Z.; Wang, T.; Lei, G.; Li, J.; Viehland, D. Direct Measurement of Magnetoelectric Exchange in Self-Assembled Epitaxial $BiFeO_3-CoFe_2O_4$ Nanocomposite Thin Films. *Appl. Phys. Lett.* **2009**, *94*, 192902.
9. Bozorth, R. M.; Tilden, E. F.; Williams, A. J. Anisotropy and Magnetostriction of Some Ferrites. *Phys. Rev.* **1955**, *99*, 1788–1798.
10. Zavaliche, F.; Zhao, T.; Zheng, H.; Straub, F.; Cruz, M. P.; Yang, P. L.; Hao, D.; Ramesh, R. Electrically Assisted Magnetic Recording in Multiferroic Nanostructures. *Nano Lett.* **2007**, *7*, 1586–1590.
11. Yan, L.; Wang, Z.; Xing, Z.; Li, J.; Viehland, D. Magnetoelectric and Multiferroic Properties of Variously Oriented Epitaxial $BiFeO_3-CoFe_2O_4$ Nanostructured Thin Films. *J. Appl. Phys.* **2010**, *107*, 064106.
12. Zheng, H.; Zhan, Q.; Zavaliche, F.; Sherburne, M.; Straub, F.; Cruz, M. P.; Chen, L. Q.; Dahmen, U.; Ramesh, R. Controlling Self-Assembled Perovskite-Spinel Nanostructures. *Nano Lett.* **2006**, *6*, 1401–1407.
13. Béa, H.; Dupé, B.; Fusil, S.; Mattana, R.; Jacquet, E.; Warot-Fonrose, B.; Wilhelm, F.; Rogalev, A.; Petit, S.; Cros, V.; *et al*. Evidence for Room-Temperature Multiferroicity in a Compound with a Giant Axial Ratio. *Phys. Rev. Lett.* **2009**, *102*, 217603.
14. Zeches, R. J.; Rossell, M. D.; Zhang, J. X.; Hatt, A. J.; He, Q.; Yang, C.-H.; Kumar, A.; Wang, C. H.; Melville, A.; Adamo, C.; *et al*. A Strain-Driven Morphotropic Phase Boundary in $BiFeO_3$. *Science* **2009**, *326*, 977–980.
15. Mazumdar, D.; Shelke, V.; Iliev, M.; Jesse, S.; Kumar, A.; Kalinin, S.; Baddorf, A.; Gupta, A. Nanoscale Switching Characteristics of Nearly Tetragonal $BiFeO_3$ Thin Films. *Nano Lett.* **2010**, *10*, 2555–2561.
16. Wojdel, J. C.; Iñiguez, J. *Ab Initio* Evidence for Giant Magnetoelectric Responses Driven by Structural Softness. *Phys. Rev. Lett.* **2010**, *105*, 037208.
17. Hatt, A. J.; Spaldin, N. A.; Ederer, C. Strain-Induced Isosymmetric Phase Transition in $BiFeO_3$. *Phys. Rev. B* **2010**, *81*, 054109, and references therein.
18. Suzuki, Y.; Hu, G.; van Dover, R. B.; Cava, R. J. Magnetic Anisotropy of Epitaxial Cobalt Ferrite Thin Films. *J. Magn. Magn. Mater.* **1999**, *191*, 1–8.
19. Gao, X. S.; Bao, D. H.; Birajdar, B.; Habisreuther, T.; Mattheis, R.; Schubert, M. A.; Alexe, M.; Hesse, D. Switching of Magnetic Anisotropy in Epitaxial $CoFe_2O_4$ Thin Films Induced by $SrRuO_3$ Buffer Layer. *J. Phys. D: Appl. Phys.* **2009**, *42*, 175006.
20. MacManus-Driscoll, J. L.; Zerrer, P.; Wang, H.; Yang, H.; Yoon, J.; Fouchet, A.; Yu, R.; Blamire, M. G.; Jia, Q. X. Strain Control and Spontaneous Phase Ordering in Vertical Nanocomposite Heteroepitaxial Thin Films. *Nat. Mater.* **2008**, *7*, 314–320.
21. Yang, H.; Wang, H.; Yoon, J.; Wang, Y.; Feldmann, D. M.; Dowden, P. C.; MacManus-Driscoll, J. L.; Jia, Q. X. Vertical Interface Effect on the Physical Properties of Self-Assembled Nanocomposite Epitaxial Films. *Adv. Mater.* **2009**, *21*, 3794–3798.
22. Sánchez, F.; Ferrater, C.; Guerrero, C.; García-Cuenca, M. V.;

Varela, M. High-Quality Epitaxial $LaNiO_3$ Thin Films on $SrTiO_3$(100) and $LaAlO_3$(100). *Appl. Phys. A: Mater. Sci. Process.* **2000**, *71*, 59–64.
23. Dix, N.; Muralidharan, R.; Warot-Fonrose, B.; Varela, M.; Sánchez, F.; Fontcuberta, J. Critical Limitations in the Fabrication of Biferroic $BiFeO_3$-$CoFe_2O_4$ Columnar Nanocomposites Due to Bismuth Loss. *Chem. Matter* **2009**, *21*, 1375–1380.
24. Muralidharan, R.; Dix, N.; Skumryev, V.; Varela, M.; Sánchez, F.; Fontcuberta, J. Synthesis, Structure, and Magnetic Studies on Self-Assembled $BiFeO_3$-$CoFe_2O_4$ Nanocomposite Thin Films. *J. Appl. Phys.* **2008**, *103*, 07E301.
25. Zheng, H.; Straub, F.; Zhan, Q.; Yang, P. L.; Hsieh, W. K.; Zavaliche, F.; Chu, Y. H.; Dahmen, U.; Ramesh, R. Self-Assembled Growth of $BiFeO_3-CoFe_2O_4$ Nanostructures. *Adv. Mater.* **2006**, *18*, 2747–2752.
26. Lüders, U.; Sánchez, F.; Fontcuberta, J. Self-Organized Structures in $CoCr_2O_4$ (001) Thin Films: Tunable Growth from Pyramidal Clusters to a {111} Fully Faceted Surface. *Phys. Rev. B* **2004**, *70*, 045403.
27. Dix, N.; Skumryev, V.; Laukhin, V.; Fàbrega, L.; Sánchez, F.; Fontcuberta, J. Sputtering Growth and Characterization of $CoFe_2O_4-BaTiO_3$ Nanostructures. *Mater. Sci. Eng., B* **2007**, *144*, 127–131.
28. Zheng, H.; Kreisel, J.; Chu, Y. H.; Ramesh, R.; Salamanca-Riba, L. Heteroepitaxially Enhanced Magnetic Anisotropy in $BaTiO_3-CoFe_2O_4$ Nanostructures. *Appl. Phys. Lett.* **2007**, *90*, 113113.
29. Zheng, H.; Growth and Characterization of Multiferroic $BaTiO_3-CoFe_2O_4$ Thin Film Nanostructures. Ph.D. Thesis, University of Maryland, 2004,http://www.lib.umd.edu/drum/handle/1903/2026; pp 104−114.
30. Li, J.;Engineering of Self-Assembled Multiferroic Nanostructures in $PbTiO_3-CoFe_2O_4$ Thin Films. Ph.D. Thesis, University of Maryland, 2006,http://www.lib.umd.edu/drum/handle/1903/3319; pp 46−74.